C. R. Palevol 16 (2017) 508–520

Contents lists available at ScienceDirect

Comptes Rendus Palevol

www.sciencedirect.com

Human Palaeontology and Prehistory (Palaeoanthropology)

Echoes from the past: New insights into the early hominin cochlea from a phylo-morphometric approach

Échos du passé : éclairages nouveaux sur la cochlée des premiers homininés par une approche phylo-morphométrique

José Braga[a,b,*], Priscille Bouvier[a,c], Jordan Romeyer Dherbey[a], Patricia Balaresque[a], Laurent Risser[d], Jean-Michel Loubes[d], Jean Dumoncel[a], Benjamin Duployer[e], Christophe Tenailleau[e]

[a] *Computer-assisted Palaeoanthropology Team, UMR 5288 CNRS, Université de Toulouse (Paul-Sabatier), 37, allées J-Guesde, 31000 Toulouse, France*
[b] *Evolutionary Studies Institute, University of Witwatersrand, 1, Jan Smuts Avenue, Braamfontein 2000, Johannesburg, South Africa*
[c] *Institut national des sciences appliquées, 135, Avenue de Rangueil, 31077 Toulouse cedex 4, France*
[d] *Statistics and Probability Team, Institute of Mathematics of Toulouse, UMR 5219 CNRS–Université de Toulouse (Paul-Sabatier), 118, route de Narbonne, 31062 Toulouse, France*
[e] *CIRIMAT, UMR 5085 CNRS–Université de Toulouse (Paul-Sabatier), 118, route de Narbonne, 31062 Toulouse, France*

ARTICLE INFO

Article history:
Received 10 October 2016
Accepted after revision 27 February 2017
Available online 18 May 2017

Handled by Roberto Macchiarelli and Clément Zanolli

Keywords:
Cochlea
Hominins
Phylogram
Brownian evolution
Australopithecus africanus
Paranthropus robustus
Homo

Mots clés :
Cochlée
Homininés
Phylogramme
Évolution brownienne

ABSTRACT

We investigate cochlear variation, an indirect evidence of auditory capacities among early hominins and extant catarrhine species, in order to assess (i) the phylogenetic signal of relative external cochlear length (RECL) and oval window area (OWA), (ii) the evolutionary model with the highest probability of explaining our observed data, (iii) some hominin ancestral nodes for RECL and OWA. RECL has a high phylogenetic signal under a Brownian motion model, and is closely correlated with body mass. Our model-based method has the advantage over parsimony-based methods of incorporating branch lengths in a phylo-morphospace, and this shows RECL shifted towards significantly higher values at the *Homo erectus-Homo sapiens* node. We also observe that the StW 53 and KB 6067 fossil specimens from Sterkfontein and Kromdraai likely represent one or two distinct, smaller-bodied and less derived hominin form(s) compared to *Paranthropus* specimens represented at Swartkrans.

RÉSUMÉ

Nous examinons la variation cochléaire, témoin indirect des capacités auditives des premiers homininés ainsi que d'espèces actuelles de catarrhiniens, afin d'évaluer (i) le signal phylogénétique de la longueur externe relative de la cochlée (RECL) et de la surface de la fenêtre ovale (OWA), (ii) le modèle évolutif montrant la plus forte probabilité d'expliquer

* Corresponding author at: Computer-assisted Palaeoanthropology Team, UMR 5288 CNRS, université de Toulouse (Paul-Sabatier), Toulouse, France.
E-mail address: jose.braga@univ-tlse3.fr (J. Braga).

http://dx.doi.org/10.1016/j.crpv.2017.02.003

Australopithecus africanus
Paranthropus robustus
Homo

nos observations, (iii) certaines valeurs ancestrales d'homininés pour RECL et OWA. RECL montre un signal phylogénétique élevé sous un modèle brownien, mais aussi une corrélation étroite avec la masse corporelle. Notre méthode, basée sur un modèle évolutif, présente l'avantage de tenir compte des longueurs de branches (contrairement aux méthodes cladistiques, basées sur la parcimonie) dans un espace phylo-morphologique soulignant une évolution de RECL vers des valeurs significativement plus élevées uniquement au nœud (*Homo erectus*, *Homo sapiens*). Nous observons également que les fossiles StW 53 et KB 6067 (provenant respectivement de Sterkfontein et de Kromdraai) représentent probablement une ou deux forme(s) d'homininé(s) de plus petite taille corporelle et moins dérivée(s), par rapport à *Paranthropus* représenté à Swartkrans.

1. Introduction

Amongst the five main sensory systems, the cochlea is the only organ that imprints details of its overall structure within bone; this takes the form of a spiral-shaped cavity housed by the petrosal part of the temporal. At least two features of this cavity can be determined and enable good estimates of the hearing capacities in fossil hominins: the relative external cochlear length (RECL) and the oval window area (OWA) (see Braga et al., 2013, 2015 for more details). For instance, cochlear length is taken as a proxy measure of a shorter basilar membrane length (with its sensors tuned to high frequencies at its base and lower frequencies progressively towards the apex), and was suggested to provide a good estimate of low-frequency hearing in non-human primates (Coleman and Colbert, 2010). One can therefore question how interactions of our hominin ancestors with environmental signals (i.e. habitat acoustics and vocalizations) may have played a role in the evolution of the unique low-frequency sensitivity displayed only by modern humans (i.e. *Homo sapiens sapiens*) among catarrhine primates (Coleman, 2009). This question is beyond the scope of the present study.

However, since cochlear features are useful in reconstructing the evolutionary history of auditory capacities among primates (Coleman and Colbert, 2010; Coleman et al., 2010), and show an association with phylogeny (Braga et al., 2015), we address two questions in this paper. First, can statistical procedures improve the detection of taxa that deviate significantly from general allometric equations (i.e. have larger or smaller cochlear features given their body size)? Second, can gross geometrical features of the cochlea in an unknown ancestral species be accurately predicted from knowledge of its phylogenetic nodal position? In order to address these issues, it is desirable to determine whether the cochlear geometrical variation observed among early hominins and other catarrhine species is phylogenetically meaningful (similarities indicating shared recent common ancestry) in possible relation to body size, and whether this can be tested according to different explicit evolutionary models (e.g., Brownian motion versus models with variable rates of evolution).

In a recent paper, Braga et al. (2015) used microfocus X-ray computed tomography (micro-ct) to measure the strength of RECL and OWA phylogenetic signals, and to determine whether some hominin species showed cochlear shifts for their body mass after correcting for gene-based phylogeny. It was concluded that RECL evolution in apes occurred mainly through body-mass-dependent and non-homoplasic changes. Moreover, both premodern and modern humans (*Homo erectus* and *H. sapiens sapiens*, respectively) showed RECL and OWA values larger than expected for their body mass (using phylogenetically controlled linear regressions), a condition not found in their non-human hominin predecessors (Braga et al., 2015). However, in that study, all the phylogenetic analyses assumed that Brownian motion was the best evolutionary model to explain the cochlear data observed among catarrhines. In a Brownian motion model of trait evolution, the expected phenotypic difference between sister species grows proportional to the time since they shared a common ancestor (i.e. the sum of the branch lengths between the two taxa) (Nunn, 2011). Given the available evidence that functional systems often do not evolve at constant rates but instead show strong positive selections (with accelerated evolutionary changes) (e.g., Clark et al., 2003), it is necessary to test whether RECL and OWA may have evolved following a non-Brownian model before attempting to reconstruct ancestral values.

Both RECL and/or OWA values have been investigated in *Australopithecus* (Sts 5, StW 329, StW 98, StW 255), *Paranthropus* (KB 6067, TM 1517, SK 879, SKW 18) and *H. erectus sensu lato* (or *H. ergaster*) (SK 847) (for more details, see Braga et al., 2013: Table 3; Braga et al., 2015: S1 table). However, since this study focuses mainly on phylogenetic issues, the KB 6067 specimen is treated separately from the Swartkrans *Paranthropus* sample because it has been preliminarily interpreted to "represent a more primitive condition for the *P. robustus* lineage, with more similarity to some Sterkfontein Member 4 specimens" (Braga et al., 2013: 455). Moreover, in the present study, we use only fossil specimens with both RECL and OWA values, hence allowing comparisons of the phylogenetic results for these two parameters by using the same samples. Therefore, Sts 5 and TM 1517 are excluded from our sample.

In addition to published data, the first aim of this study is to provide further RECL and OWA micro-ct measurements for three early hominin specimens from the Sterkfontein site (South Africa). The first, StW 498e has

been attributed to the "*Paranthropus*-like" *Australopithecus prometheus*, considered as a second species from Sterkfontein Member 4 by Clarke (2008) (for more details, see the recent review by Grine, 2013). StW 151 has been regarded as representing "a hominid more derived towards an early *Homo* condition than the rest of the *A. africanus* sample from Member 4" (Moggi-Cecchi et al., 1998; p. 462) and StW 53 has been attributed to early *Homo* (Hughes and Tobias, 1977), to *A. africanus* (Clarke, 2008; Kuman and Clarke, 2000) or to a form that is more closely affiliated to *A. africanus* than to early *Homo* (Braga, 1998).

The present study has three other main aims employing specimens representing 9 hominoid and 13 cercopithecoid extant species and their associated gene-based consensus phylogram (i.e. a phylogenetic tree with "molecular-calibrated" branch lengths) obtained using 10kTrees for Primates, V2 (http://www.10ktrees.fas.harvard.edu/) (Arnold et al., 2010). First, we explore further (as compared to Braga et al., 2015) the phylogenetic signal of RECL and OWA in extant species before and after controlling for body size. Second, we investigate whether the Brownian evolutionary model, the Ornstein–Uhlenbeck (OU) process, or the accelerating versus decelerating rates of character evolution (ACDC) best explains the observed RECL and OWA data in these species. Third, we use the evolutionary model that is most appropriate to our data (e.g., Brownian motion or Ornstein–Uhlenbeck or ACDC) to estimate some hominin ancestral conditions of RECL and OWA from a phylogram that combines data for extant and fossil species (Fig. 1; see details below).

2. Materials and methods

2.1. Micro-ct data

Table 1 presents the details of RECL and OWA values (given to the nearest one-tenth millimeter) used in the present study for each fossil hominin specimen, as well as the mean values for fossil and extant species.

Most of the micro-ct measurements used in this study were employed previously by Braga et al. (2015) (see Table S1 for more details) with isometric voxel dimensions ranging from 7.0 to 41 microns (μm). Therefore, we do not repeat here the details about the samples and the body mass data already given in Braga et al. (2015). Additional measurements of RECL and OWA were taken from the micro-cts of 7 *Gorilla gorilla* skulls (from specimens housed at the "Musée royal de l'Afrique centrale", Tervuren, Belgium; with only one of them of known sex) obtained using the Nanotom (GE Sensing) at the "Fédération de recherche" FERMAT (CIRIMAT, Toulouse) (all with isometric voxel dimensions of 32.6 μm). The micro-ct data for StW 498e, StW 151 and StW 53 were obtained in South Africa using the XTH 225/320 LC dual source system (Nikon) at the Palaeosciences Centre, University of the Witwatersrand,

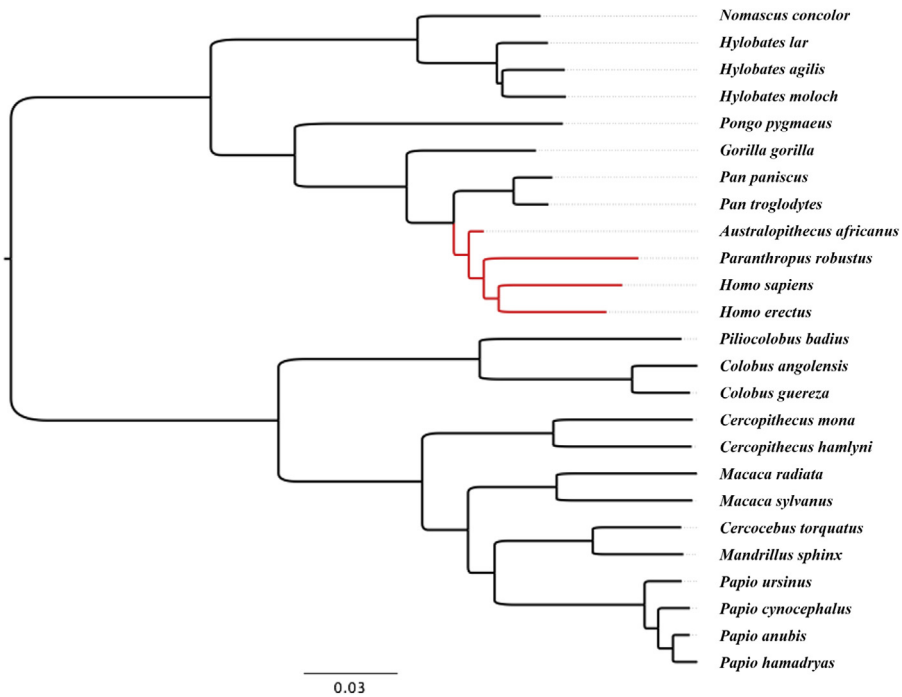

Fig. 1. Phylogram for 22 extant catarrhine species and three extinct hominin species made from grafting the tree for the extinct hominins using morphology onto the extant molecular tree.
Fig. 1. Phylogramme pour 22 espèces actuelles de catarrhiniens et trois espèces d'homininés fossiles, construit en greffant l'arbre des fossiles établi par la morphologie sur celui obtenu par les données moléculaires.

Table 1
Micro-ct relative external cochlear length (RECL) and oval window area (OWA) mean values for extant and fossil species, and measurements for fossil hominin specimens. Voxel sizes are indicated in microns.
Tableau 1
Valeurs moyennes de RECL and OWA pour les espèces actuelles et fossiles, et mesures individuelles pour les hominiés fossiles, obtenues par microtomographies. Les dimensions des *voxel sizes* sont indiquées en microns.

	RECL	OWA	Voxel size
Homo erectus			
SK 847 (R)	14.2	3.3	21.7
Paranthropus (*n* = 3)	14.3	4.1	
SK 879 (L)	14.8	4.3	9.2
SKW 18 (R)	13.8	3.9	11.1
KB 6067	11.8	2.8	7.4
Australopithecus (*n* = 6)	12.5	2.6	
StW 329	11.8	2.0	33.1
StW 98	12.7	3.1	33.1
StW 255	12.8	2.8	33.1
StW498e	13.3	2.0	28.1
StW53g	12.3	2.5	30.5
StW151c	12.2	3.4	28.3
Homo sapiens (*n* = 22)	14.6	3.7	41.0
Pan troglodytes (*n* = 9)	13.3	3.1	41.0
Pan paniscus (*n* = 7)	12.5	2.5	8.0–41.0
Gorilla gorilla (*n* = 14)	14.6	3.9	32.6–41.0
Pongo pygmaeus (*n* = 8)	13.6	4.0	12.0–41.0
Nomascus concolor (*n* = 1)	9.7	1.6	41.0
Hylobates moloch (*n* = 1)	10.2	1.8	41.0
Hylobates lar (*n* = 1)	10.9	1.5	9.0
Hylobates agilis (*n* = 2)	10.4	1.6	7.3–8.3
Papio hamadryas (*n* = 2)	10.5	1.6	41.0
Papio cynocephalus (*n* = 5)	10.4	1.4	7.8-41.0
Papio ursinus (*n* = 1)	11.0	1.6	41.0
Papio anubis. (*n* = 2)	11.8	1.5	8.1-8.6
Mandrillus sphinx (*n* = 1)	11.2	1.6	41.0
Macaca radiata (*n* = 1)	9.6	0.9	41.0
Macaca sylvanus (*n* = 2)	9.5	1.3	41.0
Cercopithecus mona (*n* = 1)	9.8	1.2	41.0
Cercopithecus hamlyni (*n* = 1)	9.1	1.1	41.0
Cercocebus torquatus (*n* = 1)	10.3	1.5	41.0
Colobus angolensis (*n* = 3)	10.2	1.4	7.0–41.0
Colobus guereza (*n* = 4)	10.0	1.3	41.0
Piliocolobus badius (*n* = 4)	9.8	1.0	41.0

Johannesburg, with isometric voxel dimensions ranging from 28.1 to 30.5 μm.

2.2. Measurement protocol for OWA

The micro-ct measurement methodology of RECL and OWA is detailed in Braga et al. (2015). Moreover, we illustrate the micro-ct measurement protocol used in this study for OWA with an example taken for the *P. robustus* SK 879 specimen (Fig. 2). This example is motivated in part by the difficulties expressed in the literature about accurate measures of the oval window in the narrow oval window niche (*fenestra vertibuli*), a variably deep depression located partly behind the overhanging and prominent promontory of the tympanic cavity (*promontorium tympani*) (Fig. 2). In a detailed analysis of the stapes footplate, Sim et al. (2013) stated that measurements taken on photographs "might not be the most precise way of measuring the dimensions of the ossicles" (op. cit., p. 160). Noussios et al. (2016) also considered that photographic measurements of the stapes footplate in the oval window niche may entail errors regarding the projection of such a small surface into a screen (parallax error). Since several studies now consider in situ micro-ct measurements of the middle ear as more accurate and efficient than measurements taken on photographs (this point will be discussed in more details below), we prioritize micro-cts to measure OWA in fossil hominins and extant catarrhines (Braga et al., 2013, 2015).

We first visualized (by using the Avizo solftware. https://www.fei.com/software/amira-avizo/) the oval window niche in 3D after extracting an isosurface from the micro-ct data set, as shown in Fig. 2a with the case of SK 879. We then defined an oblique slice that best-fitted the complete outline of the oval window at the location of the annular stapedial ligament, a ring of fibrous tissue that connects the oval window to the stapes footplate. The OWA was then measured from its segmentation on this oblique slice. Since we used high resolution micro-ct data (Table 1), the outline of the insertion area of the annular stapedial ligament could be visualized accurately. This allowed us to reduce to a minimum (less than 5%) the interobserver variability between two operators (J.B. and J.R.D.) in setting an oblique slice in the plane of the OWA.

2.3. The maximum likelihood framework

All the phylogenetic methods and tests presented below have been implemented by using the statistical maximum likelihood (ML) framework that was first introduced for phylogenetic studies by Edwards and Cavalli-Sforza (1964) for gene frequency data. The application of ML to phylogenies involves searching for the single tree (i.e. a topology with branch lengths) that, under a given evolutionary model, best explains the observed data (i.e. the traits for each species, for more details, see Baum and Smith, 2013). In doing so, it is conventional to record the logarithm of the likelihood, the log-likelihood (to avoid problems associated with handling very small numbers) of that tree as the main criterion.

An important point to stress here is that analyses for morphological data are still often based on parsimony, a method that is less computationally demanding and "consistent if the rate of evolutionary change per branch of the tree is sufficiently small" (Felsenstein, 2004:122). Intuitively speaking, the statistical property of parsimony (for more details, see Felsenstein, 2004) means that it minimizes the number of changes that have occurred in each branch and therefore assumes a low rate of change (i.e. fewer evolutionary events, so the phylogram will show relatively shorter branch lengths in all characters). Moreover, the advantage of ML methods over parsimony analysis is that the former use information on branches lengths available in phylograms. Given the fact that different characters are often expected to evolve at different rates and that longer branches offer more opportunities for changes to occur than shorter branches, ML methods are particularly useful in this context. We use freely available packages (listed below) in the R Statistical Computing environment http://www.r-project.org/. These packages are summarized in the CRAN project: http://www.cran.r-project.org/web/views/Phylogenetics.html.

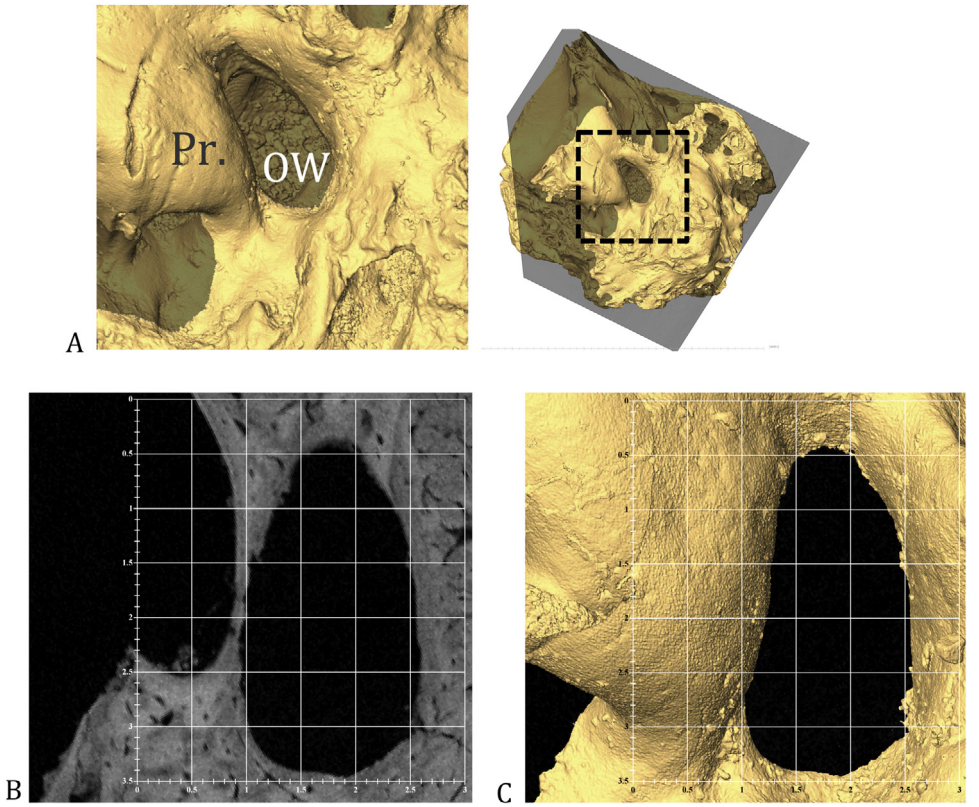

Fig. 2. 3D reconstruction from micro-ct data of the middle ear cavity of SK 879 (A); oblique slice used to measure oval window area (OWA) and superimposed on a grid of 0.5 × 0.5 mm uniformly distributed squares (B); and 3D view of the oval window niche (C) using exactly the same viewpoint, magnification, grid and orientation as in B.
Fig. 2. Reconstruction 3D à partir de données micro-tomographiques, de la cavité de l'oreille moyenne de SK 879 (A) ; coupe oblique utilisée pour mesurer OWA et superposée à une grille composée de carrés de 0,5 mm de côté (B) ; et vue 3D de la niche de la fenêtre ovale (C) en utilisant exactement les mêmes points de vue, grossissement, grille et orientation que pour B.

2.4. The phylogenetic signal

We first investigate whether the cochlear data observed for extant species derive from a nonrandom, gene-based tree-like descent process. The basic principle is to determine whether a given tree derived from genetic distances better fits a set of cochlear data (as represented by species mean values) at its tips, when compared with the fit obtained when the cochlear data have been randomly permuted across the tips of the tree, thus destroying any phylogenetic signal that may have existed. We investigate the phylogenetic signal in this dataset before and after controlling for body size. We use distinct R packages to compare two estimates of the phylogenetic signal for RECL and OWA considered separately: the λ of Pagel (1999) the *K* of Blomberg (Blomberg et al., 2003).

Pagel's (1999) λ is a parameter multiplied to each of the off-diagonal elements of the variance-covariance matrix (see Nunn, 2011, for more details). When λ = 0, the tree has a single polytomy at the basal node for all species, whereas when λ = 1 the original candidate tree is recovered. Statistical tests for phylogenetic signal are performed under the null hypothesis that λ = 0. Tests for less signal than the candidate tree are performed under the null hypothesis that λ = 1. We compute Pagel's λ with the R package "Geiger" (its function "fitContinuous") under the assumption of a Brownian model of evolution (see below). We also compute Pagel's λ with the R package "Caper" (its function "pgls") with no prior assumption about any given model of evolution. In all instances, we test our null hypotheses with the likelihood ratio (LR) test (twice the log-likelihood difference between the two models is expected to fit a Chi^2 distribution with *P* degrees of freedom) (Baum and Smith, 2013; Nunn, 2011).

We compute Blomberg's *K* statistic (Blomberg et al., 2003) with the R "Picante" and "Ape" packages in order to test also whether the observed distributions for RECL and OWA across catarrhine species exhibit more or less divergence than expected when evolving under Brownian motion. Values of *K* range from 0 to infinity, with *K* = 1 indicating Brownian motion evolution. *K* > 1 indicates that close relatives are more similar than expected, and *K* < 1 indicates more divergence between taxa than expected under a Brownian model. In order to decide whether the calculated *K* value corresponds to a Brownian model, we test if it is significantly higher than the mean *K* value obtained after simulating 1000 datasets (i.e. trees) with random permutations of the tips.

We also use phylogenetic generalized least squares (PGLS) (with the "pgls" function of the R package "Caper") to

assess whether either RECL or OWA considered separately may have undergone correlated evolution with body mass (BM). Therefore, we estimate the slopes of RECL versus BM and OWA versus BM regressions, and test whether these slopes are significantly different from 0. We subsequently calculate the phylogenetic signal of RECL and OWA after allometric correction (i.e. removing the allometric effect of body mass here represented by mean species values).

2.5. Choosing an evolutionary model

In this part of the study, we aimed to characterize the tempo (or rate) and the mode (the mechanisms) of RECL and OWA evolutionary changes by testing which evolutionary model best explains the observed data. We consider the following three evolutionary models: BM, OU and ACDC.

We first consider the Brownian motion (BM) model assuming that rates of evolution are constant over time (i.e. larger changes more likely occur on longer branches). Therefore, this model was also called "constant variance process" (Freckleton et al., 2002; Pagel, 2002). In this model, the instantaneous phenotypic variance σ^2 per unit time t (i.e. the change along a branch of length t, or rate of change) is drawn from a normal distribution with mean 0 and variance σ^2 t. Therefore, the trait variance is proportional to time (or branch length) and the displacements in different branches of a tree are independent. It is important to add here that the BM model does not necessarily indicate neutral or random evolution. It can instead reflect adaptive evolutionary changes (Nunn, 2011).

In contrast to BM, the Ornstein–Uhlenbeck (OU) model can be viewed as acting to limit evolutionary variation. Indeed, it is biologically unrealistic to consider that the range of a trait value could vary infinitely. The OU model can therefore be applicable when traits likely evolved with constraints on their maximum or minimum values, depending on the strength of stabilizing selection (Felsenstein, 1988; Garland et al., 1993). It is a BM model pulled to include one or more selective optima that assert an attractive force on Brownian trait evolution. When the strength of this attraction is zero, the OU model is identical to a BM model. Very strong stabilizing selection can obliterate the effects of history such that phylogenetic signal disappears. In this event, trait values will be more similar in closely or distantly related species experiencing the same selective pressures.

The acceleration or deceleration (ACDC) of Brownian motion evolution from the root to the tips of the tree is the third model used in this study. The ACDC model (also called "early burst") describes evolution that either increases (accelerates, AC) or decreases (decelerates, DC) in rate over time.

We choose the evolutionary model that best describes the species data sampled in our study with the use of LR tests and the Akaike information criterion (AIC) (Akaike, 1974). The model with the smallest AIC is the preferred one. We also use the corrected AIC (AICc) for small samples.

2.6. Estimates of ancestral values

We estimate RECL and OWA ancestral values (using the preferred evolutionary model chosen in the previous step) at internal nodes of a phylogeny reconstructed with morphological and molecular data by grafting a tree for three extinct hominin species of known cochlear values (*A. africanus*, *P. robustus* and *H. erectus*) onto the gene-based phylogram representing contemporaneous catarrhine species (Fig. 1). The extinct hominin phylogram (i.e. branch lengths proportional to the amount of evolutionary change) is obtained from Organ et al. (2011) and was inferred using 109 morphological characters from Strait and Grine (2004) in a Bayesian framework.

We use the R package "Phytools" (and its "fastAnc" function) (Revell, 2012) to compute ancestral values and 95% CIs (to reflect uncertainty) using ML (i.e. finding values that maximize the probability of our data). We consider that our approach is unbiased because we use the evolutionary model that best fits our data. The ability of different methods (e.g., ML under different models of evolution) to accurately estimate ancestral values and their associated errors has been investigated by Martins (1999), who showed that a BM model performed reasonably well, especially for more recent ancestors. Therefore, in order to reduce uncertainty, we limit our estimates for hominin ancestral nodes that are close to the tips (as opposed to those that are deeper in the tree). We consider the following four nodes: (*Pan*, *Hominins*), (*A. africanus*, *P. robustus*, *Homo*), (*P. robustus*, *Homo*) and (*H. erectus*, *H. sapiens*) (Fig. 1).

3. Results

3.1. Variation of RECL and OWA among early hominins

We first represent in a simple 2D-point graph, the variation of RECL versus OWA among early hominins, *H. sapiens sapiens*, *Gorilla gorilla* and *Pan troglodytes*/*paniscus* (Fig. 3). At first glance, we observe a clear separation between a group comprising the four *Australopithecus* specimens from Sterkfontein (StW 498e, StW 255/259, StW 98 and StW 329), StW 53, StW 151 and KB 6067, and a second group made up of *P. robustus* from Swartkrans (SK 879 and SkW 18) and *H. erectus* (SK 847) with noticeably higher values for both RECL and OWA (Fig. 3). In this regard, it is important to note that RECL is a better discriminator than OWA, the SK 847 OWA value falling within the variability sampled for specimens derived from Sterkfontein Member 4. We also observe that *H. sapiens* and *Gorilla gorilla* specimens overlap one another and that most of them have higher values of RECL than that for *Pan troglodytes*/*paniscus*. While the three specimens of *P. robustus* from Swartkrans and *H. erectus* group fall within *H. sapiens* and *Gorilla gorilla* ranges, all the other fossil hominins sampled here from Kromdraai and Sterkfontein group with values for *Pan troglodytes*/*paniscus*. Moreover, the StW 329 specimen shows remarkably low RECL and OWA values.

3.2. Phylogenetic signal of RECL and OWA

For both RECL and OWA, we obtain a high Pagel's λ that is significantly different from 0 but notdifferent from 1,

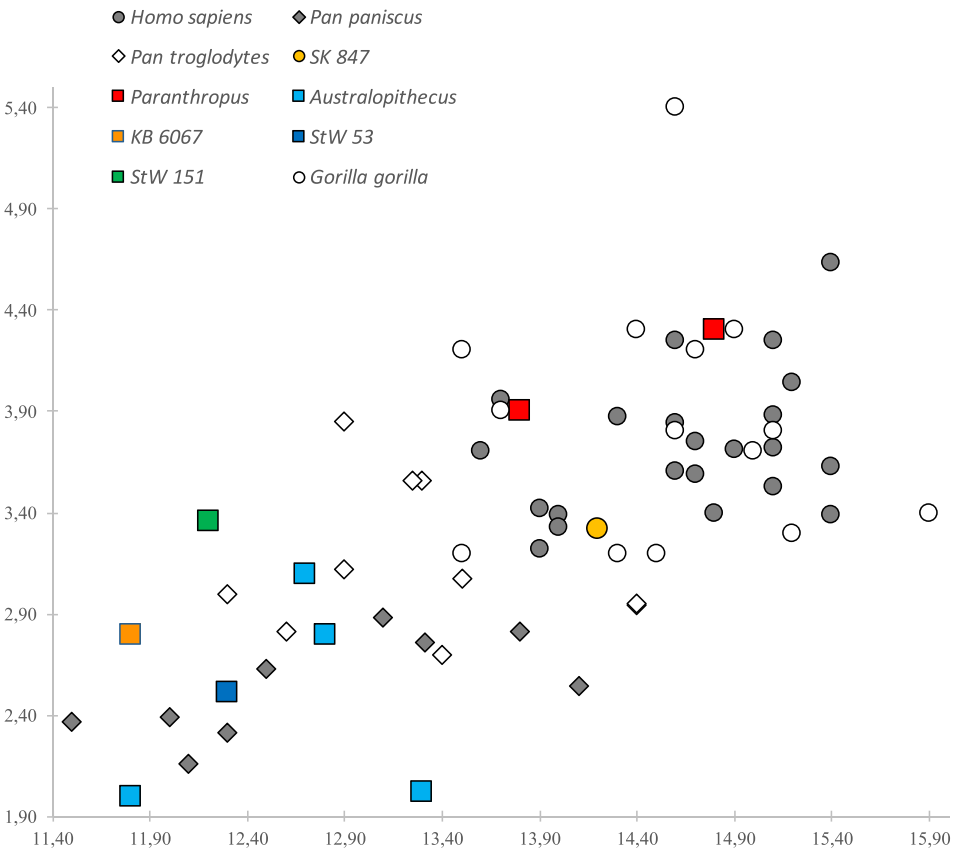

Fig. 3. 2D-point graph representing relative external cochlear length (RECL) and oval window area (OWA) values in fossil hominins, *Homo sapiens*, *Pan* and *Gorilla*.
Fig. 3. Graphique 2D de nuage de points représentant les valeurs de RECL et OWA chez les homininés fossiles, *Homo sapiens*, *Pan* et *Gorilla*.

Table 2
Phylogenetic signals as represented by the λ of Pagel and the *K* of Blomberg for relative external cochlear length (RECL) and oval window area (OWA), before and after correction for body mass (BM), under a standard Brownian motion model of evolution. The results of the log-likelihood ratio tests, the permutation tests (*K* mean) and the Akaike information criterion (AIC) (with the corrected AIC–AICc for small samples) are also detailed. ML for maximum likelihood.
Tableau 2
Signaux phylogénétiques représentés par les λ de Pagel et *K* de Blomberg pour RECL et OWA, avant et après correction allométrique par la masse corporelle (BM), sous un modèle d'évolution brownien standard. Les résultats des tests de *ratio* de log-vraisemblances, des tests de permutation (*K* mean) et critères d'Akaike (AIC) (valeur AIC–AICc corrigée pour les petits échantillons) sont également détaillés. ML pour maximum de vraisemblance.

	RECL	OWA	BM
λ of Pagel (ML, Brownian, Geiger)	0.926133	1.000000	
λ of Pagel (ML, Caper)	0.926000	1.000000	1.0000
Log-likelihood ratio	40.089887	18.966384	–
	–	–	
AIC	−74.179773	−31.932767	–
	–	–	
AICc	−72.846440	−30.599434	–
	–	–	
P-value 5% (different from 0) (Geiger)	2.060154e-05	4.523477e-07	
P-value 5% (different from 0) (Caper)	2.0602e-05	4.5236e-07	4.8937e-06
P-value 5% (different from 1) (Geiger)	0.1446526	1	
P-value 5% (different from 1) (Caper)	0.14465	1	1
K Blomberg	0.9848426	1.522079	1.229131
K mean (1000)	0.0001673756	0.001036746	
P-value	0.000999001	0.000999001	
Pagel: BM (Caper)	0.320	0.735	
P-value 5% (different from 0)	0.10004	0.0003707	
P-value 5% (different from 1)	0.0014589	0.029203	

either under the assumption of a Brownian model of evolution, or with no prior assumption about any given model of evolution (Table 2). The same trend is observed when we compute the Blomberg's *K* statistic. In all instances, the *K* values are significantly higher than those obtained randomly and indicate either Brownian motion evolution (RECL; $K = 0.98$) or closer relatives more similar than expected (OWA; $K = 1.52$) (Table 2).

Since BM shows a high phylogenetic signal for both Pagel's λ (significantly different from 0, but not from 1) and Blomberg's *K* (1.22) (Table 2), it is important to investigate whether RECL and OWA still show a high phylogenetic signal after controlling for BM. We obtain a low Pagel's λ (0.32; not significantly different from 0) for RECL after controlling for BM ($r^2 = 0.78$, $P < 0.005$). For OWA, after controlling for BM ($r^2 = 0.68$; $P < 0.005$), the Pagel's λ is higher than for RECL, with a value (0.735) significantly different from 0, but not different from 1 at 0.03% (Table 2).

3.3. Choice of an evolutionary model for RECL and OWA

We first compute the log-likelihood for a Brownian model of evolution for RECL and OWA considered separately (Table 3). We then compute the log-likelihoods for OU and ACDC models of evolution of RECL and OWA in order to determine whether one of them better explains our observed data than Brownian motion. Both LR tests and AIC criteria (either AIC or AICc) show that the evolutionary model that best explains the data (i.e. RECL and OWA values and the gene-based phylogram) observed in extant species is Brownian motion (Table 3). This model is therefore used for ancestral states reconstructions.

Table 3
Log-likelihoods, LR tests and AIC (AICc) criteria for three distinct models of evolution for relative external cochlear length (RECL) and oval window area (OWA): Brownian motion model, Ornstein–Uhlenbeck model and ACDC or "early burst" model.
Tableau 3
Log-vraisemblances, tests de *ratio* de log-vraisemblances, et critères d'Akaike (AIC et AICc) pour trois modèles d'évolution distincts de RECL et OWA : modèle brownien, modèle d'Ornstein–Uhlenbeck et modèle ACDC ou *early burst*.

	RECL	OWA
Brownian motion model		
Log-likelihood	39.026010	18.966384
AIC	−74.052020	−33.932767
AICc	−73.420441	−33.301188
Ornstein–Uhlenbeck model		
Log-likelihood	39.076838	18.966384
AIC	−72.153675	−31.932767
AICc	−70.820342	−30.599434
P-value	0.7498513	1
ACDC or "early burst" model		
Log-likelihood	39.026003	19.583036
AIC	−72.052007	−33.166072
AICc	−70.718674	−31.832739
P-value	1	0.2667654

3.4. Ancestral states reconstructions

Since both RECL and OWA show high phylogenetic signals (when considered separately), we estimate the ancestral values (with 95% CIs) of these two parameters at the three hominin nodes in the phylogram (Fig. 1), as well as at the *Pan*-Hominin node (Figs. 4 and 5).

With regard to RECL, there is a clear trend for an increase of the ancestral values from the oldest node (*Pan*, *Hominins*)

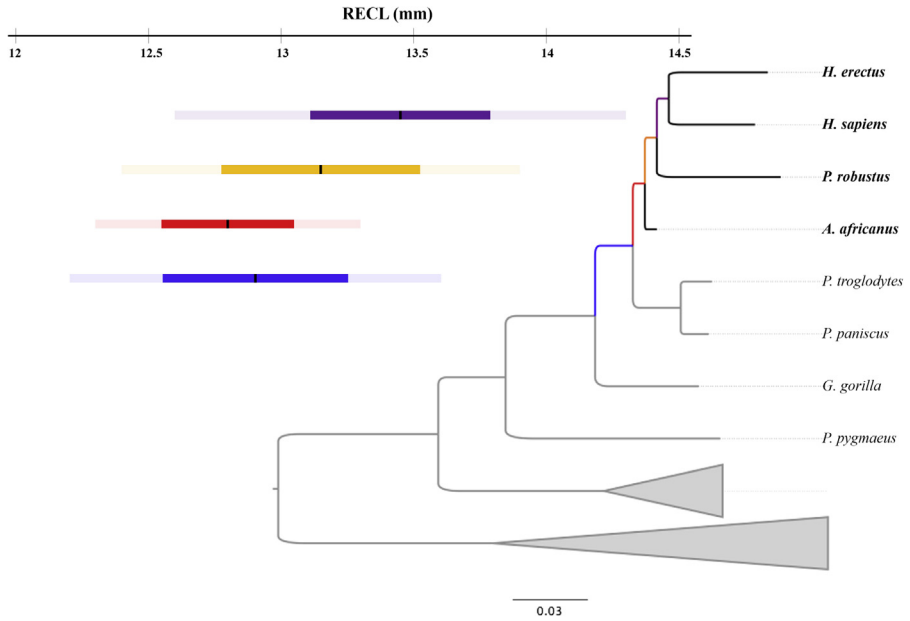

Fig. 4. Ancestral values for relative external cochlear length (RECL) estimated at the (*Pan*, *Hominins*) (blue), (*A. africanus*, *P. robustus*, *Homo*) (red), (*P. robustus*, *Homo*) (yellow) and (*H. erectus*, *H. sapiens*) (violet) nodes. The confidence intervals are illustrated with one standard deviation (with two standard deviations in transparency).
Fig. 4. Valeurs ancestrales de RECL estimées aux nœuds (*Pan*, *Hominins*) (bleu), (*A. africanus*, *P. robustus*, *Homo*) (rouge), (*P. robustus*, *Homo*) (jaune) et (*H. erectus*, *H. sapiens*) (violet). Les intervalles de confiance sont illustrés avec une déviation standard (avec deux déviations standard en transparence).

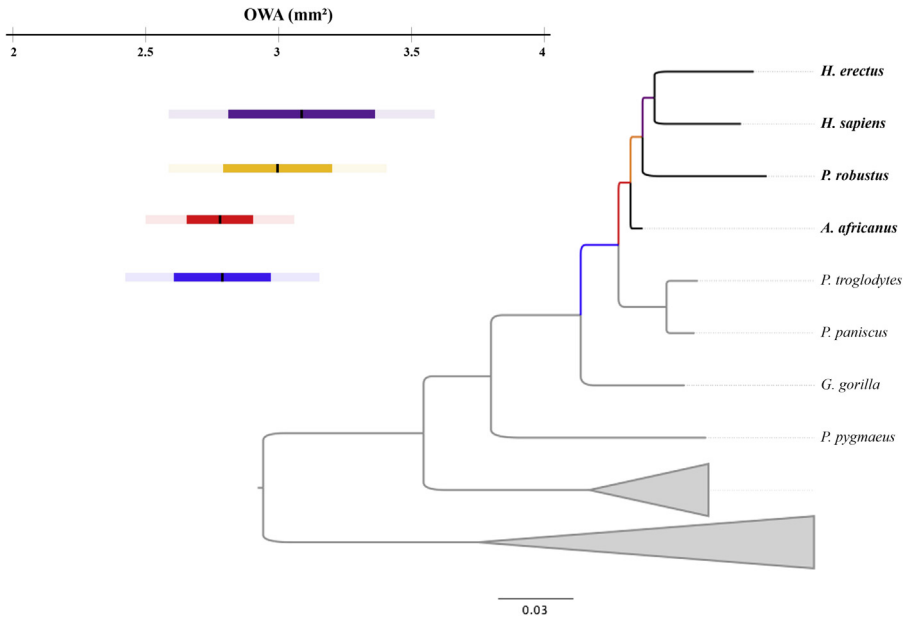

Fig. 5. Ancestral values for oval window area (OWA) estimated at the (*Pan*, *Hominins*) (blue), (*A. africanus*, *P. robustus*, *Homo*) (red), (*P. robustus*, *Homo*) (yellow) and (*H. erectus*, *H. sapiens*) (violet) nodes. The confidence intervals are illustrated with one standard deviation (with two standard deviations in transparency).

Fig. 5. Valeurs ancestrales de OWA estimées aux nœuds (*Pan*, *Hominins*) (bleu), (*A. africanus*, *P. robustus*, *Homo*) (rouge), (*P. robustus*, *Homo*) (jaune) et (*H. erectus*, *H. sapiens*) (violet). Les intervalles de confiance sont illustrés avec une déviation standard (avec deux déviations standard en transparence).

to the youngest one and (*H. erectus*, *H. sapiens*) (Fig. 4). The (*A. africanus*, *P. robustus*, *Homo*) node's CI at 95% fits completely within the (*Pan*, *Hominins*) node's CI at 95%. Moreover, the (*P. robustus*, *Homo*) and (*H. erectus*, *H. sapiens*) nodes' RECL estimations fall outside the (*A. africanus*, *P. robustus*, *Homo*) node's CI at 63% (i.e. with only one standard deviation) and 95%, respectively. There is no overlap between the (*A. africanus*, *P. robustus*, *Homo*) and the (*H. erectus*, *H. sapiens*) nodes' CIs at 63% (Fig. 4).

There is also a trend for an increase of the OWA ancestral values from the oldest node (*Pan*, *Hominins*) to the youngest one (*H. erectus*, *H. sapiens*) (Fig. 5). As for RECL, the (*A. africanus*, *P. robustus*, *Homo*) node's CI at 95% is encompassed by the (*Pan*, *Hominins*) node's CI at 95%. However, there is more overlap between the three OWA hominin nodes' CIs at 63% (Fig. 5) than for RECL (Fig. 4). In particular, there is an almost complete overlap between the (*A. africanus*, *P. robustus*, *Homo*) and the (*H. erectus*, *H. sapiens*) nodes' CIs at 63% (Fig. 5).

In order to evaluate the impact on estimates of RECL and OWA ancestral values when grafting a tree for three extinct hominin species onto the gene-based phylogram representing extant species only, we computed the (*Pan*, *Homo*) node CIs before the incorporation of fossil data (as in Braga et al., 2015). For both RECL and OWA, the (*Pan*, *Homo*) nodes' CIs at 95% (12.5–14.7 mm and 2.6–3.9 mm^2, respectively) were almost identical to the (*H. erectus*, *H. sapiens*) nodes' CIs obtained from the tree combining extant and fossil species (Figs. 4 and 5). This result demonstrates the usefulness of grafting fossil tip data onto the gene-based phylogenetic tree for ancestral reconstructions at some nodes.

4. Discussion

In order to better interpret our fossil cochlear parameters, we aimed to use our dataset representing contemporaneous catarrhine species to (i) explore further the phylogenetic signal before and after controlling for body size, (ii) investigate whether the Brownian model is appropriate when modeling cochlear evolution and (iii) estimate some fossil hominin ancestral conditions of RECL and OWA from a phylogram combining extant and fossil data. Here, we discuss only the taxonomic and phylogenetic aspects of our results since direct transcriptions of fossil hominin RECL and OWA differences into hearing capabilities and communication signals would be premature for the following reasons. Indeed, previous studies in living great apes have demonstrated the complexity of calling behaviors on primate sound and vocal repertoires as, for instance, within highly variable call types (e.g., long vocalizations) variations in acoustic structure, call repertoire size correlated with group size and social bonding, socially learned calls and divisions of calls according to home range (Harcourt and Stewart, 2001; Hardus et al., 2009; Marshall et al., 1999).

4.1. RECL and OWA estimates in fossil hominins

Apart from Braga et al. (2013, 2015), we could not find any other RECL measurements in early hominins to compare with ours. Moreover, we discuss below why we consider that the micro-ct OWA measurements presented here are not interchangeable with published measurements of the oval window or stapes footplate area taken on scaled digital images in fossil hominins (e.g., Quam et al.,

2015). Quam et al. (2015) assessed photographically the OWA or the stapes footplate area and considered that, in all instances (i.e. for all fossil specimens), the latter represented 90% of the former. If we use this 90% proportion to compare the micro-ct OWA values in fossil hominins presented in this study (Table 1) and the photographic measurements published in Quam et al. (2015, Table 1) (e.g., the stapes footplate area of SKW 18 or the OWA of SK 879), we observe marked discrepancies (except for STW 328), in particular for *P. robustus*. Here we take one example presented in Fig. 2 in order to briefly discuss this point. The most important discrepancy (1.6 mm^2) is observed for the SK 879 specimen illustrated with an oblique slice that best-fits the complete outline of its OWA (Fig. 2B) and with a 3D view of its oval window niche (Fig. 2C). As shown in a comparison between Fig. 2B and C, the configuration of the oval window niche poses two main difficulties when trying to measure the small OWA with no parallax error.

The first difficulty is due to the fact that, even when the middle ear cavity is visually accessible without endoscopy (as for SK 879), the promontory of the tympanic cavity prevents the visualization of the complete outline of the oval window to allow for an accurate photographic measurement of OWA to the nearest one-hundredth square millimeter with no potential parallax error. This potential parallax error explains why in situ micro-ct measurements of middle ear features have been considered as more accurate than photographic measurements (e.g., Noussios et al., 2016; Sim et al., 2013).

The second difficulty is related to the need for a perfect calibration of the photograph to be used for accurate measurements of OWA. First, the scale used for calibration needs to be placed at precisely the same distance from the camera lens as the oval window itself. Moreover, if a millimeter ruler scale is used, it needs to fit inside the narrow oval window niche next to the OWA (Fig. 2C), and also to lie exactly in its plane (i.e. the OWA and the ruler scale need to be co-planar). Small misalignment and/or placement errors of the ruler scale will result in uncertainties on the calibration of the photograph used for measurements.

In the case of the SK 879 micro-ct data, we obtained a 4.3-mm^2 OWA value (Table 1). In Fig. 2B, we superimpose a grid of 0.5 × 0.5 mm uniformly distributed squares (with surface areas of 0.25 mm^2 each) over the oblique slice that we used to obtain this OWA value for SK 879. Fig. 2C shows exactly the same viewpoint, magnification and orientation of this specimen as in Fig. 2B. The same grid is superimposed on a 3D endo-tympanal view of the SK 879 oval window niche. A visual comparison shows a noticeable difference between Fig. 2B and C in the measure of the OWA with at least 0.5 mm^2 (2 squares). As shown here, such a difference is due to the overhanging promontory of the tympanic cavity that could be also seen in a photograph or under a microscope. Moreover, the grid superimposed on the OWA of the SK 879 specimen (Fig. 2B) allows the reader to visually assess that its value is close to 4.0 mm^2. A 2.43-mm^2 value was given in Quam et al. (2015) for the SK 879 estimated stapes footplate area. If we assume that the stapes footplate represented 90% of the OWA in SK 879 (as suggested in Quam et al., 2015), we obtain a 2.7-mm^2 value. This measurement is incompatible with the micro-ct value (4.3 mm^2) that we repeatedly obtained for SK 879 after careful segmentations (Fig. 2).

Another important point to discuss is the correspondence between the stapes footplate area and the OWA. The difference between these two areas is due to the size of the annular ligament of the stapes. In a detailed micro-CT measurement study of the annular ligament of the human stapes, Mohammadi et al. (2016) found it highly variable in its volume and thickness. Because of this variability among modern humans, we would urge caution when estimating OWA from the stapes footplate area in other extant species, as well as in fossil hominins with a single constant proportion. The proportion of 90% used for fossil hominins in Quam et al. (2015) likely represents only the upper part of the variation of the relationship between OWA and the stapes footplate area. Here, we argue that more comparative micro-CT measurements of the OWA and the stapes footplate area are needed in both modern humans and other extant catarrhines for better estimations of measurements errors when assessing the former variable from the latter. Indeed, from the micro-ct data of the middle ear obtained by one of us (J.B.), we observe a 76–87% variability (caused by interindividual differences and lateral asymmetry) in the proportion of the OWA represented by stapes footplate area in only 12 measurements for modern humans. This observation is well in line with the results presented in Mohammadi et al. (2016). Moreover, when we investigate the proportion of the OWA represented by the stapes footplate area using our micro-ct data for 11 specimens representing non-human primate species, we observe a range between 79% (*Papio hamaryas*) and 90% (*Pongo pygmaeus*).

4.2. Exploring new basicranial features

The present study confirms, using additional tests, the very high phylogenetic signal of RECL and OWA parameters and their close correlation with body mass, as already observed by Braga et al. (2015). Moreover, we newly observe that a Brownian motion model is the best evolutionary framework to compare RECL and OWA differences between catarrhine species, including fossil hominins. Importantly, while RECL evolution is associated with evolutionary changes in body mass, OWA likely evolved more independently. Therefore, comparisons between fossil hominin specimens and species based on RECL and OWA may lead to reliable identifications of monophyletic groups with their associated synapomorphies (as opposed to homoplasies).

The fossil cochlear values presented here confirm the RECL distinctiveness of the *Paranthropus* and *H. erectus* specimens found at Swartkrans compared to the *Australopithecus* specimens from Sterkfontein (Braga et al., 2013, 2015). The *Paranthropus* and *H. erectus* RECL values are similar to measurements for extant humans and gorillas, but also noticeably higher to those for any specimen from Sterkfontein, including StW 151 or StW 53 (Fig. 3). Interestingly, the StW 53 RECL and OWA values appear very close to those recently published for KB 6067, a juvenile fossil hominin from the South African site of Kromdraai (Braga

et al., 2013, 2016) which has been attributed to an evolutionary less derived *P. robustus* form than that represented at Swartkrans. Indeed, as noted by Braga et al. (2013), StW 53 and KB 6067 also appear similar in the morphology of their semi-circular canals. Interestingly, while StW 53 and StW 151 petrous bones have been regarded as very close in morphology and more like the modern human condition than exhibited by other Sterkfontein specimens, the OWA size in StW 53 falls in the range of *P. paniscus* whereas the much larger OWA of StW 151 falls in the range of both *H. sapiens* and *G. gorilla.* Moreover, the RECL values of both StW 53 and StW 151 fall well below the *P. robustus. H. erectus* and *H. sapiens* values (Fig. 3).

As indicated in Braga et al. (2013), the taxonomic attribution of KB 6067 from Kromdraai Member 3 is as yet unclear. A firmer taxonomic attribution of the oldest Kromdraai paranthropines (including KB 6067) is still pending on the analysis of the larger hominin sample discovered in the oldest fossiliferous deposits from this site (Braga and Thackeray, 2016; Braga et al., 2017). This will allow us to determine whether the southern African *Paranthropus* hypodigm represents either a single and variable *P. robustus* species with a time span yet unknown, or distinct taxa (i.e. at most the more plesiomorphic *P. robustus* from Kromdraai and *P. crassidens* from Swartkrans; at least a single evolutionary *P. robustus* species consisting in a lineage of ancestral descendant populations; for more details, see Braga et al., 2016, 2017). Further discoveries combined with progress in measuring the complex cochlear shape will allow us to test whether the variable OWA and RECL signatures obtained between Swartkrans (e.g., SKW 18 and SK 879) and Kromdraai (e.g., KB 6067) paranthropines are consistent with "a plesiomorphic status of the KB hominins, indicative of their ancestral status for the *P. robustus* + *boisei* clade, giving rise before 2.3 Ma to the split of *P. boisei* in East Africa and *P. robustus* survivors in South Africa" (Braga et al., 2016:65).

Even though our results are preliminary, given the phylogenetic tests presented here and their advantage over parsimony-based interpretations (see below), we argue that StW 53 and KB 6067 may represent one or two distinct smaller-bodied, less derived hominin form(s), as compared to *Paranthropus* and *H. erectus* specimens represented at Swartkrans. We acknowledge that labyrinthine similarities are not sufficient to establish firm taxonomic affiliations and that our conclusions need to be tested by further comparative morphological studies. For instance, although the spiraled shape of the cochlea appears globally similar among catarrhines, the development of new 3D morphometric methods may uncover taxonomic distinctions because its spiraled structure makes it inefficient to study with standard Euclidian metrics.

The base of the cranium has often been considered evolutionarily more conservative that the face and teeth (Bosma, 1976; de Beer, 1937; Lieberman et al., 1996; Strait, 1998; Strait et al., 1997). Variations in the cranial base other than those investigated here (e.g., the angle of the petrous part of the temporal bone to the coronal plane) have been considered useful in phylogenetic analyses (Dean, 1986; Dean and Wood, 1981), but have not been tested using the statistical methods employed here. In line with our results, these basicranial features have been regarded as distinct between the contemporaneous great apes and *Australopithecus*, on the one hand, and *Paranthropus* and *Homo* on the other. Further comparative data and investigations at both intra- and inter-specific levels in extant and fossil taxa will improve our phylogenetic interpretations, and in particular, we need data on the cochlear variability in highly dimorphic hominid species such as *G. gorilla*. As yet, we only investigated the RECL variability in a *G. gorilla* sample of very limited size ($n = 14$) and with most specimens ($n = 12$) of unknown sex ($n = 12$) and two males.

4.3. Paranthropus and Homo shared features

On the basis of the high phylogenetic signal of RECL and OWA and our evolutionary model-based phylogenetic statistics, here we interpret the *P. robustus* and *Homo* shared and derived cochlear features reported on Swartkrans specimens (i.e. higher values for both RECL and OWA) as synapomorphies. From our very limited sample of fossil hominins and the results presented in Figs. 4 and 5, it is tempting to suggest a *A. africanus* to *P. robustus* ancestral-descendant relationship. However, such a conclusion would be unwise if it rests only on high RECL and OWA phylogenetic signals. We nevertheless argue that the improvement of our understanding of the phylogenetic relationships between the southern African paranthropines and other early hominin taxa, including early *Homo* and *Paranthropus* from East Africa, depends on further analyses of the skull base, including the morphology of the cochlea.

As yet, the cranial base flexion has garnered a lot of attention and, to the best of our knowledge, its derived morphology shared between *Homo* and *Paranthropus* has not been explored among fossil and extant primates using phylogenetically informed statistical analyses. Even though we used such analyses in the present cochlear study, we cannot yet determine whether the RECL and OWA derived features shared between *P. robustus* and *Homo* at Swartkrans are also shared with eastern African *Paranthropus* and *Homo*. There is no consensus on the basal species leading to *Paranthropus* and *Homo*, depending on the phylogenetic role accorded to *A. africanus* and *P. aethiopicus* (Strait and Grine, 2004) and *Paranthropus* phylogeny (Wood and Constantino, 2007, fig. 10). Therefore, more comparative studies on *Australopithecus* and *Paranthropus* specimens from southern and eastern Africa will be needed to decide whether *A. africanus* represents the most likely common ancestor of *P. robustus* and *Homo*, *Paranthropus* and *Homo* or if an alternative scenario is more likely.

In line with results from Baker et al. (2016) and the positive selection associated with shifts in molar area relative to body size in *Paranthropus*, our phylogenetic findings support a significant role of selection in shaping the evolution of *P. robustus* and *Homo* auditory capacities, at least as represented by RECL (Fig. 4). The positive association between BM and RECL observed in this study (see also Braga et al., 2015) means that there is an evolutionary correlation between BM and cochlear size among catarrhines, including fossil hominins. Since RECL does not show

a phylogenetic signal significantly different from 0 after controlling for BM, the ancestral values proposed here highlight, at least partly, the role of selection on a larger body size in shaping cochlear evolution in *Homo*. Only further measurements of RECL in fossil *Homo* specimens will allow us to determine the exact shifts in cochlear size relative to body size during the earliest part of the evolution of our genus. The use of a phylogram combining extant and fossil species to estimate ancestral RECL values at three hominin nodes in this study (Fig. 4), confirms a previous finding that RECL is "hypertrophied" in the genus *Homo*, as opposed to the australopiths (*Australopithecus* and *Paranthropus*) (Braga et al., 2015). Indeed, when RECL is represented in a phylo-morphospace (Fig. 4), the (*H. erectus*, *H. sapiens*) nodes' value is clearly shifted towards a higher RECL, as compared to the ancestral value at the (*P. robustus*, *Homo*) node. Moreover, when we consider the OWA parameter with its high phylogenetic signal after correcting for BM (contrary to RECL), we observe that OWA values are shifted towards higher values at the (*P. robustus*, *Homo*) node. Further estimates of ancestral node values will be needed to help refining the predictions by adding new fossil hominin species values at the tips of the tree used in the statistical analyses. To this end, cochlear investigations on *A. afarensis*, *P. aethiopicus* and *P. boisei* will be crucial.

4.4. Cladistic versus phylogenetic methods

The present study demonstrates that a simple Brownian model of evolution best explains the observed RECL and OWA data in contemporaneous species. Therefore, this model assuming constant rates of evolution over time is appropriate for ancestral reconstructions. Moreover, this result highlights the importance of investigating cochlear changes among fossil hominins by using an evolutionary framework with stretched and compressed branch lengths that conforms to our assumed underlying Brownian motion mode. Such an evolutionary framework is more realistic because it assumes that changes in character values are more likely along longer branches, i.e. over longer stretches of time. When branch lengths are available, our proposed model-based method has the advantage of incorporating these data. By contrast, the parsimony-based methods used for cladistics reconstructions assume that changes are equally likely on all branches of the tree, regardless of their length. This assumption would be safe only for very slowly evolving traits, but not for cochlear evolution among hominins. In this context, methods using parameters with a measured phylogenetic signal (i.e. statistically tested using a phylogenetic comparative approach) will be very useful to investigate further the hypothesized *Paranthropus* monophyly (see reviews in Wood and Boyle, 2016; Wood and Constantino, 2007), its diversification into eastern and southern African forms from a common ancestor often set during the 2.7–2.3 Ma period, and its phylogenetic relationships with the origin of our own genus *Homo*.

Acknowledgments

We take this opportunity to share our memories of Laurent Puymerail who was a magnificent and resourceful young colleague. Laurent's contributions and personality will remain with us for a long time to come. We thank Roberto Macchiarelli and Clément Zanolli for their invitation to contribute to this thematic issue in honor of Laurent Puymerail's work.

This work was supported by the the French Ministry of Foreign Affairs, the "Centre national de la recherche scientifique" and its "Projet exploratoire pluridisciplinaire inter-instituts" PEP II-AUDEVO in France, the South African National Research Foundation. We thank Emmanuel Gilissen from the "Musée royal de l'Afrique centrale" (Tervuren, Belgium), Bernhard Zipfel and the Fossil Access Committee, from the University of the Witwatersrand (Johannesburg, South Africa) for giving us access to the specimens newly investigated in this study. We are also grateful to Kristian Carlson and Jakata Kudakwashe for their help with the scanning of three fossil hominin specimens from Sterkfontein (South Africa). These data were produced at the Palaeosciences Centre Microfocus X-ray Computed Tomography (CT) Facility at the University of the Witwatersrand. We finally deeply thank Frederick Grine, one anonymous reviewer and Roberto Macchiarelli (associate editor) for their very helpful comments, which improved the manuscript.

References

Akaike, H., 1974. A new look at the statistical model identification. IEEE Trans. Autom. Control. 19, 716–723.

Arnold, C., Matthews, L.J., Nunn, C.L., 2010. The 10kTrees Website: a new online resource for primate phylogeny. Evol. Anthropol. 19, 114–118.

Baker, J., Meade, A., Pagel, M., Venditti, C., 2016. Positive phenotypic selection inferred from phylogenies. Biol. J. Linn. Soc. 118, 95–115.

Baum, D.A., Smith, S.D., 2013. Tree thinking. An introduction to phylogenetic biology. Roberts and Co, Greenwood Village.

Blomberg, S., Garland, T., Ives, A., 2003. Testing for phylogenetic signal in comparative data: behavioral traits are more labile. Evolution 57, 717–745.

Bosma, J.F., 1976. Development of the Basicranium. National Institutes of Health, Bethesda, Maryland.

Braga, J., 1998. Chimpanzee variation facilitates the interpretation of the incisive suture in South African Plio-Pleistocene hominids. Am. J. Phys. Anthropol. 105, 121–135.

Braga, J., Thackeray, J.F., 2016. Kromdraai. A birthplace of *Paranthropus* in the cradle of humankind. Sun Press, Johannesburg, South Africa.

Braga, J., Thackeray, J.F., Dumoncel, J., Descouens, D., Bruxelles, L., Loubes, J.-M., Kahn, J.-L., Stampanoni, M., Bam, L., Hoffman, J., de Beer, F., Spoor, F., 2013. A new partial temporal bone of a juvenile hominin from the site of Kromdraai B (South Africa). J. Hum. Evol. 65, 447–456.

Braga, J., Loubes, J.-M., Descouens, D., Thackeray, J.F., Dumoncel, J., Kahn, J.-L., de Beer, F., Riberon, A., Hoffman, K., Balaresque, P., Gilissen, E., 2015. Disproportionate cochlear length in genus *Homo* shows a high phylogenetic signal during apes' hearing evolution. PLoS One 10, e0127780.

Braga, J., Dumoncel, J., Duployer, B., Tenailleau, C., de Beer, F., Thackeray, J.F., 2016. The Kromdraai hominins revisited with an updated portrayal of differences between *Australopithecus africanus* and *Paranthropus robustus*. In: Braga, J., Thackeray, J.F. (Eds.), Kromdraai. A birthplace of *Paranthropus* in the cradle of humankind. Sun Press, Johannesburg, pp. 49–68.

Braga, J., Thackeray, J.F., Bruxelles, L., Dumoncel, J., Fourvel, J.-B., 2017. Stretching the time span of hominin evolution at Kromdraai (Gauteng, South Africa): Recent discoveries. C.R. Palevol 16, 58–70.

Clark, A., Glanowski, S., Nielsen, R., Thomas, P.D., Kejariwal, A., Todd, M.A., Tanenbaum, D.M., Civello, D., Lu, F., Murphy, B., Ferriera, S., Wang, G., Zheng, X., White, T.J., Sninsky, J.J., Adams, M.D., Cargill, M., 2003. Inferring nonneutral evolution from human-chimp-mouse orthologous gene trios. Science 302, 1960–1963.

Clarke, R.J., 2008. Latest information on Sterkfontein's *Australopithecus* skeleton and a new look at *Australopithecus*. S. Afr. J. Sci. 104, 443–449.

Coleman, N.M., 2009. What do primate hear? A meta-analysis of all known non-human primate behavioral audiograms. Int. J. Primatol. 30, 55–91.
Coleman, M.N., Colbert, M., 2010. Correlations between auditory structures and hearing sensitivity in nonhuman primates. J. Morph. 27, 511–532.
Coleman, M.N., Kay, R.F., Colbert, M.W., 2010. Auditory morphology and hearing sensitivity in fossil new world monkeys. Anat. Rec. 293, 1711–1721.
Dean, M.C., 1986. *Homo* and *Paranthropus*: similarities in the cranial base and the developing dentition. In: Wood, B.A., Martin, L.B., Andrews, P. (Eds.), Major topics in primate and human evolution. Cambridge University Press, Cambridge, pp. 249–265.
Dean, M.C., Wood, B.A., 1981. Metrical analysis of the basicranium of extant hominoids and *Australopithecus*. Am J Phys Anthropol 54, 53–71.
de Beer, G.R., 1937. The development of the vertebrate skull. Oxford University Press, Oxford.
Edwards, A.W.F., Cavalli-Sforza, L.L., 1964. Reconstruction of evolutionary trees. Phenetic and phylogenetic classification. Syst. Assoc. Publ. 6, 67–76.
Felsenstein, J., 1988. Phylogenies from molecular sequences: inferences and reliability. Ann. Rev. Genet. 22, 521–565.
Felsenstein, J., 2004. Inferring phylogenies. Sinauer Associates, Sunderland.
Freckleton, R.P., Harvey, P.H., Pagel, M., 2002. Phylogenetic analysis and comparative data: a test and review of evidence. Am. Nat. 160, 712–726.
Garland Jr., T., Dickerman, A.W., Janis, C.M., Jones, J.A., 1993. Phylogenetic analysis of covariance by computer simulation. Syst. Biol. 42, 265–292.
Grine, F.E., 2013. The alpha taxonomy of *Australopithecus africanus*. In: Reed, K.E., Fleagle, J.G., Leakey, R.E. (Eds.), The paleobiology of *Australopithecus*. Springer, New York, pp. 73–104.
Harcourt, A.H., Stewart, K.J., 2001. Vocal relationships of wild mountain gorillas. In: Robbins, M.M., Sicotte, P., Stewart, K.J. (Eds.), Mountain Gorillas: three decades of research at Karisoke. Cambridge University Press, Cambridge, UK, pp. 241–262.
Hardus, M.E., Lameira, A.R., Singleton, I., Morrogh-Bernard, H.C., Knott, C.D., Ancrenaz, M., Utami Atmoko, S.S., Wich, S.A., 2009. A description of the orangutan's vocal and sound repertoire, with a focus on geographic variation. In: Wich, S.A., Utami Atmoko, S.S., Mitra Setia, T., van Schaik, C.P. (Eds.), Orangutans. Geographic variation in behavioral ecology and conservation. Oxford University Press, Oxford, UK, pp. 49–64.
Hughes, A.R., Tobias, P.V., 1977. A fossil skull probably of the genus *Homo* from Sterkfontein. Transvaal. Nat. 265, 310–312.
Kuman, K., Clarke, R.J., 2000. Stratigraphy, artefact industries and hominid associations for Sterkfontein, Member 5. J. Hum. Evol. 38, 827–847.
Lieberman, D.E., Pilbeam, D.R., Wood, B.A., 1996. Homoplasy and early *Homo*: an analysis of the evolutionary relationships of *H. habilis sensu stricto* and *H. rudolfensis*. J. Hum. Evol. 30, 97–120.
Marshall, A.J., Wrangham, R., Clark Arcadi, A., 1999. Does learning affect the structure of vocalizations in chimpanzees? Anim. Behav. 58, 825–830.
Martins, E.P., 1999. Estimation of ancestral states of continuous characters: a computer simulation study. Systematic Biology 48, 642–650.
Moggi-Cecchi, J., Tobias, P.V., Beynon, A.D., 1998. The mixed dentition and associated skull fragments of a juvenile fossil hominid from Sterkfontein, South Africa. Am. J. Phys. Anthropol. 106, 425–466.
Mohammadi, A., Jufas, N., Sale, P., Lee, K., Patel, N., O'Leary, S., 2016. Micro-CT analysis of the anatomical characteristics of the stapedial annular ligament. Anat. Sci. Int., 1–15, http://dx.doi.org/10.1007/s12565-016-0331-4.
Noussios, G., Chouridis, P., Kostretzis, L., Natsis, K., 2016. Morphological and morphometrical study of the human ossicular chain: a review of the literature and a meta-analysis of experience over 50 years. J. Clin. Med. Res. 8, 76–83.
Nunn, C.L., 2011. The comparative approach in evolutionary anthropology and biology. The University of Chicago Press, Chicago.
Organ, C., Nunn, C.L., Machanda, Z., Wrangham, R.W., 2011. Phylogenetic rate shifts in feeding time during the evolution of *Homo*. Proc. Natl. Acad. Sci. U S A 108, 14555–14559.
Pagel, M., 1999. Inferring the historical patterns of biological evolution. Nature 401, 877–884.
Pagel, M., 2002. Modelling the evolution of continuously varying characters on phylogenetic trees. In: MacLeod, N., Forey, P.L. (Eds.), Morphology, shape and phylogeny. CRC Press, Boca Raton, FL, USA, pp. 269–286.
Quam, R., Martinez, I., Rosa, M., Bonmati, A., Lorenzo, C., de Ruiter, D.J., Moggi-Cecchi, J., Conde Valverde, M., Jarabo, P., Menter, C.G., Thackeray, J.F., Arsuaga, J.-L., 2015. Early hominin auditory capacities. Sci. Adv. 1, e1500355.
Revell, L.J., 2012. Phytools: an R package for phylogenetic comparative biology (and other things). Methods Ecol. Evol. 3, 217–223.
Sim, J.H., Röösli, C., Chatzimichalis, M., Eiber, A., Huber, A.M., 2013. Characterization of stapes anatomy: investigation of human and guinea pig. JARO 14, 159–173.
Strait, D.S., (Ph.D. Dissertation) 1998. Evolutionary integration in the hominid cranial base. Stony Brook, State University of New York.
Strait, D.S., Grine, F.E., 2004. Inferring hominoid and early hominid phylogeny using craniodental characters: the role of fossil taxa. J. Hum. Evol. 47, 399–452.
Strait, D.S., Grine, F.E., Moniz, M.A., 1997. A reappraisal of hominid phylogeny. J. Hum. Evol. 32, 17–82.
Wood, B.A., Constantino, P., 2007. *Paranthropus boisei:* fifty years of evidence and analysis. Yearb. Phys. Anthropol. 50, 106–132.
Wood, B.A., Boyle, E.K., 2016. Hominin taxic diversity: fact or fantasy? Yearb. Phys. Anthropol. 159, S37–S78.